Publication P1

Ville Renvall, Raimo Joensuu, and Riitta Hari. 2006. Functional phantom for fMRI: a feasibility study. Magnetic Resonance Imaging, volume 24, number 3, pages 315-320.

Available online at www.sciencedirect.com

SCIENCE DIRECT®

Magnetic Resonance Imaging 24 (2006) 315–320

MAGNETIC RESONANCE IMAGING

Functional phantom for fMRI: a feasibility study

Ville Renvall[a,*], Raimo Joensuu[a,1], Riitta Hari[a,b]

[a]Advanced Magnetic Imaging Centre, Helsinki University of Technology, P.O. Box 3000, FI-02015 TKK Espoo, Finland
[b]Brain Research Unit, Low Temperature Laboratory, Helsinki University of Technology, FI-02015 TKK Espoo, Finland

Received 17 March 2005; accepted 8 July 2005

Abstract

Functional magnetic resonance imaging (fMRI) reveals changes in blood oxygen level-dependent (BOLD) signal after considerable processing. This paper describes the implementation and testing of an fMRI phantom where electric current applied to a thin wire within a proton-rich medium substituted BOLD distortion of the magnetic field; the scanner detects these two distortions as practically identical signal changes. The magnitude of the change depended on the current strength. The phantom has a number of possible applications. Signal changes across sessions, days, instruments and individuals could be monitored. Placing the phantom close to a subject during an fMRI experiment could allow differentiating sensitivity changes in the scanner due to instrumentation from changes in the subject's state and performance during the experiment. The spatial extent of brain activations and effects of various changes in the chain of image formation could be analyzed using current-induced "activations". Furthermore, the phantom could expedite fMRI sequence development by reducing the need to scan human subjects, who introduce uncertainty to the signal. Thus, this fMRI phantom could be useful for both cognitive fMRI studies and scanner calibration.

Keywords: fMRI; BOLD; Simulation; Phantom; Calibration

1. Introduction

Functional magnetic resonance imaging (fMRI) is an indirect way to collect information on neuronal function in the brain. The hemodynamic response related to electric signaling can be measured because the magnetic susceptibility, χ_m, of oxygen-depleted blood is higher than that of fully oxygenated blood [1]; this is the basis of functional contrast in blood oxygenation level-dependent (BOLD) fMRI [2]. Changes in intensities of image elements (voxels), resulting from varying local susceptibilities inside the tissue and veins, have enabled brain activation mapping with fMRI.

fMRI activations are usually illustrated as color blobs superimposed on the structural images of the subject's brain. These blobs reveal the statistical significance of changes in the BOLD signal related to some stimuli or tasks, compared with a control condition.

The size of the voxel defines the best possible spatial accuracy available in the measurement. In the ideal case, activation inside one single voxel would stay within the single voxel also after the whole signal analysis procedure, with no changes in the neighboring voxels. In practice, the hemodynamic changes often extend over several voxels, but there are equipment- and method-related sources of apparent activation spread that are not linked to actual physiological responses and thus should not affect the activation results.

The signal acquisition method of magnetic resonance imaging (MRI) leads to unavoidable signal leakage from one voxel to its neighbors: in echo planar imaging (EPI), for example, the point-spread function is characterized by the convolution of the modulus of a sinc function with the resonance peak that is typically Lorentz-shaped; the width depends on the effective transverse relaxation time, T_2* [3]. The extent of a point-like activation's spread also depends on gradient nonlinearities, shimming and the radiofrequency (RF) electronics, on the signal processing and image analysis methods, as well as on the applied imaging parameters and scanner settings, often calibrated automatically. Thus an originally (ideal) point-like signal change

* Corresponding author. Tel.: +358 9 4516163; fax: +358 9 4516172.
E-mail address: ville@neuro.hut.fi (V. Renvall).
[1] Present address: AstraZeneca R&D Molndal, Mölndal, Sweden.

0730-725X/$ – see front matter © 2006 Elsevier Inc. All rights reserved.
doi:10.1016/j.mri.2005.07.012

may, in the final result, have spread to several neighboring voxels in a manner not routinely retrieved as a result of imaging. For proper interpretation, it would be highly beneficial to be able to discern which of the observed changes is due to changes in the subject's state and which is due to effects of data acquisition. If such information were available, one might try to optimize the imaging parameters for each experiment.

The effects of fMRI data analysis and post-processing methods on the obtained results can be studied in a rather straightforward manner by modifying digitally the time series of MR signals or by using simulated data [4,5]. Quality assurance routines of fMRI laboratories often include time series measurements with a structural phantom to study the temporal stability of the Fourier-transformed signal intensity and also to determine the system's noise level by using several techniques (e.g., the method proposed by Weisskoff [6]). Application of these methods is based on the assumption that the performance of the scanner remains stable during fMRI experiments that take place at a later time and with a different object/subject.

The quality of the baseline signal of the fMRI experiment can be evaluated, for example, by monitoring the signal intensity of a tissue whose properties stay stable during the experiment (e.g., subcutaneous fat), or by placing a small reference phantom close to the subject so that both are visible in the same image frames. The latter method is an improvement over the phantom-only technique because the stability of the baseline, and possibly also the noise level, can be determined during the actual fMRI experiment.

In a real fMRI experiment, the BOLD signal intensity variation between the rest and activation states may vary during the examination due to combined physiological and nonphysiological reasons. Similarly, the BOLD signal may differ between successive experiments despite identical imaging setups. The change in the system's sensitivity to detect the BOLD activation may remain unnoticed by available methods.

To remediate those monitoring problems, we designed and constructed an fMRI phantom; see Ref. [7] for initial results presented in abstract form. Instead of blood oxygenation changes, our phantom uses electric current in distorting the magnetic field homogeneity. Others [8] have recently introduced a different functional phantom, where the MRI signal within the phantom changes as the Q values of resonant coils are remotely adjusted, which enables enhancement (focusing) of the MR signal. Our design was inspired by earlier studies in which electric current within a sample was imaged [9,10] and used to visualize catheters in MRI [11]. Here we extend the principle to provide a tool for studying scanner sensitivity to field homogeneity changes. Consequently, our phantom adds to the possibilities of analyzing the whole chain of fMRI data formation from acquisition to brain activation mapping.

2. Methods

2.1. Analogy between BOLD and phantom-induced signal changes

BOLD signal variation is caused by local variations in magnetic susceptibility in tissues and veins. Although the MRI scanner does not directly measure field inhomogeneities, BOLD signal variation can be observed from the signal decay caused by loss of phase coherence of spins in T_2*-weighted imaging, such as gradient-recalled echo (GRE) EPI [3]. The resulting (f)MRI signal, the voltage induced into the receiver coils during transverse spin relaxation of the protons in the sample, is affected by any local field inhomogeneity, whatever its physical cause. Thus the scanner detects similarly the shortening of T_2* introduced by inhomogeneities of the static polarizing magnetic field of the scanner, local changes in susceptibility, as well as other causes of field inhomogeneities. Electric current, too, induces magnetic field, which is the mechanism producing field inhomogeneity in our fMRI phantom.

BOLD and current-induced spin-phase distortions differ qualitatively. In the brain, BOLD susceptibility changes distort the field homogeneity in and near veins and capillaries, which leads to irregular and scattered field inhomogeneities throughout the hemodynamically active tissue. On the contrary, the current-induced field produces smoothly varying field inhomogeneity within the affected volume. In effect, the current-induced distortion affects the whole volume inspected, whereas the BOLD effect might distort only the subvolume in and near veins and capillaries and therefore some baseline signal could remain completely unaltered. Furthermore, whereas the current-induced field is additive to the external field, $\mathbf{B}_{tot}(\mathbf{r},t)=\mu\mathbf{H}_{ext}+\mathbf{B}_{cur}(\mathbf{r},t)$, the BOLD effect is multiplicative: $\mathbf{B}_{tot}(\mathbf{r},t)=\mu(\mathbf{r},t)\mathbf{H}_{ext}$, where $\mathbf{B}_{tot}(\mathbf{r},t)$ is the total magnetic flux density as a function of location $\mathbf{r}$ at time t, μ is the magnetic permeability of the sample, $\mathbf{H}_{ext}$ is the external magnetic field intensity including the strong polarizing field and gradients, and $\mathbf{B}_{cur}$ is the current-induced magnetic flux density. For a phantom, the additive nature is actually practical because possible spatial variation in background signal does not propagate to different images.

Water protons in the tissue near oxyhemoglobin and deoxyhemoglobin molecules have equal chemical shifts, but their spatial encoding during MR imaging differs because of the external field variation caused by the susceptibility effect. Because the χ_m of deoxygenated red blood cells is greater than that of plasma, which in turn exceeds that of oxygenated red blood cells [12], the MR signal of water in deoxygenated blood shifts mostly in the direction of the positive low-bandwidth (phase-encoded) gradient, whereas the MR signal of water in fully oxygenated blood shifts slightly toward the negative gradient, with respect to undisturbed plasma. Therefore, near the relevant voxel border, the BOLD phase difference does not cause signal

void within the voxel, but the signal is misregistered into the neighboring voxel.

The same phenomenon occurs also for the current-induced effect: the proton MR signals near the phase-encoded border of a voxel may shift into the neighboring voxels, or signals from the neighboring voxels may shift into the voxel considered, depending on the polarity of the induced magnetic field.

2.2. fMRI phantom

Fig. 1 shows the constructed fMRI phantom. The shell of the phantom was made of a polymethylacrylate tube of 12 mm inner diameter, and the tube was filled with proton-rich rapeseed oil. A lacquer-insulated electric wire, wound tightly as a twisted pair, was fixed along the longitudinal central axis of the phantom. A container, made of 2-mm-thick copper pipe, was attached to one end of the phantom to enclose the electronic equipment, including a fiber-optic receiver, a frequency-to-voltage converter and a current driver. The power supplied to these components from outside the measurement room was filtered capacitively within the container and at the feed-through of the RF shield of the measurement room.

Pulse-frequency modulation of a fiber-optic link was used in transmitting the programmed current patterns from a computer to the phantom. A stimulus-presentation software (Presentation v. 0.76, Neurobehavioral Systems, Albany, CA, USA) was used to control the current in the wire.

The twisted pair was wound of resistive carbon fibers (92 Ω resistance along the 45-cm length of the wire) to reduce the level of RF pickup (the transverse diameter of both helices, i.e., the distance between the wires is 1.2 ± 0.3 mm, with curvature of 0.8 ± 0.1 revolutions/cm). The protons of the filling oil served as the source of the MR signal; the χ_m of vegetable oil is close to that of H_2O, i.e., only $1.55\cdot10^{-6}$ higher according to Ref. [13].

Fig. 2 shows the longitudinal (z) component of the magnetic field, B_z, computed for the twisted pair with the Biot–Savart law, assuming an infinitesimal conductor thickness. For both the 0.3- and 1.3-mA currents, the magnitude of B_z is less than a microtesla within 1 mm from the wires, and it decreases as a function of distance from the axis of the helices, d, approximately as d^{-2}. This wiring geometry produces spatially well-bound magnetic fields, where the steepest gradients, important for dephasing, stay limited to a small volume close to the twisted wire. Also, the discontinuities in the magnetic field simulations occur in

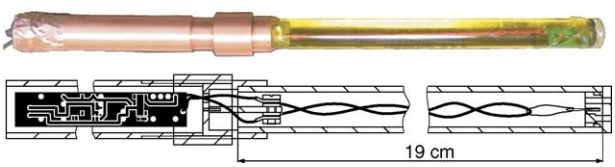

Fig. 1. The fMRI phantom. (Top) A photograph of the phantom. (Bottom) The circuit board for electronics (left) and a schematic of the liquid-filled wire-containing phantom (right).

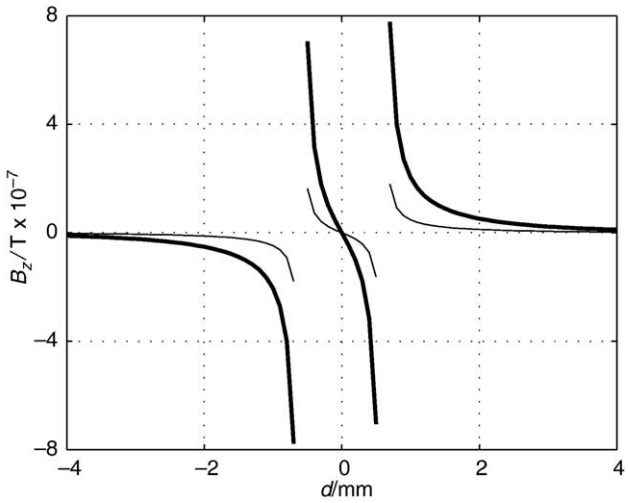

Fig. 2. Magnetic flux density induced in the z-direction by 0.3- and 1.3-mA currents (thin and thick lines, respectively) flowing in two helices. The distance d is measured from the axis of the helices and the field profile is from the cross section, including the field extrema in the transverse plane. The singular points at the wire positions do not contribute to the MR signal due to the lack of MRI-active nuclei. The immediate vicinity of the wires is covered with the insulating layer, also passive in MRI.

regions devoid of hydrogen atoms in the phantom and therefore do not contribute to the MRI signal. It is important to note, though, that the locus of the twisted wire within the volume described by an image voxel may affect the image intensity of the voxel and its neighbor, and the effect is qualitatively described here. If the high (low) B_z induced by the phantom current (see Fig. 2) coincides with the low (high) B_z border of the voxel in the phase-encoded direction, signal dislocation may result. Especially, if the wire is near the low B_z border the result may be statistically significant at the single-voxel level. The space of a voxel occupied by the wire does not contribute to the MR signal and therefore that voxel has a smaller intensity than the surrounding voxels. If any kind of field inhomogeneity injects an additional signal to this voxel from the neighbors, the relative change in image intensity is greater than for voxels containing only the proton-rich medium.

The difficulty of prescribing optimal slices in subvoxel scale can be detrimental for activation studies, as well as for attempts to calibrate the sensitivity of the scanner to field inhomogeneities. However, in the case of the fMRI phantom the lack of MR-active nuclei at and near the wires is beneficial since the peaks of the current-induced B_z are cut out and only moderate fields are effective for the protons of the background medium. Thereby only the voxels neighboring the wire-containing voxel can affect or be affected noticeably by the current-induced field. Consequently, any phantom-induced spatial misregistration is probably small. Moreover, the pixel size used in fMRI studies is usually much larger than the wires' cross-sectional dimensions, and smoothing spatial filters, which are used in most fMRI studies, will further reduce the misregistration error. In calibration measurements, still more robustness for the

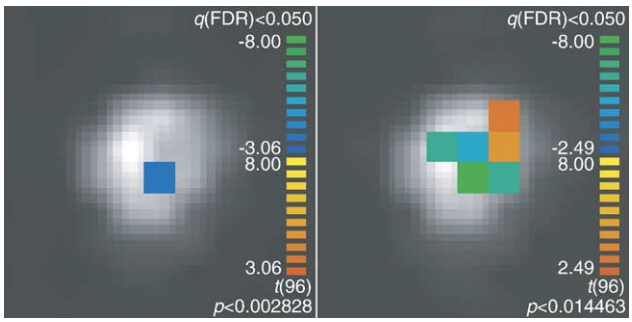

Fig. 3. Activations produced by the fMRI phantom (shown as light grey) with two current levels; the in-plane sizes of the colored squares representing activated pixels are 3.125×3.125 mm^2. In both experiments, 30-s current-on and current-off periods were repeated five times. The current was either 0.3 mA (left panel) or 1.3 mA (right panel). The image plane was selected arbitrarily, being the same in both panels, and the results were similar in all image planes. The activation maps superimposed on single GRE-EPI images are thresholded similarly with respect to the false discovery rate. The FDR is controlled at 5%, meaning that, on average, ≥95% of the shown activations are real. Color scales for Bonferroni-corrected *t*-statistics and the threshold *P* values are shown as well.

method is achieved by choosing a fair-sized region-of-interest (ROI) and averaging over it.

2.3. Experiments

The performance of the fMRI phantom was tested with a 3-T MR scanner (General Electric Signa VH/i 3.0 T MRI whole-body scanner, GE Medical Systems, Waukesha, WI, USA) equipped with a standard transmit/receive head coil. All scans were acquired with identical slice thickness (3.1 mm), gap between slices (1.0 mm), flip angle (90°), pulse repetition time (3 s), echo time (30 ms), field of view (20×20 cm^2) and number of excitations per scan (1). GRE-EPI sequence was used, and the image planes were perpendicular to the phantom's axis and also to the static polarizing field of the scanner. Three different experiments are described below.

Experiment 1 was conducted to determine whether the phantom would produce activations that can be observed with ordinary fMRI analysis software when the theoretical subvoxel field variation, caused by the current in the phantom wire, is similar to BOLD variation. The typical fMRI matrix size of 64×64 was used, resulting in an in-plane resolution of 3.125×3.125 mm^2; thus the twisted pair of wire at the centre of a voxel could fit within one voxel in the plane with a fair margin. The current in the wire was varied between two levels (I_{high} and I_{low}) once every 30 s for altogether 300 s. In the successive runs, the current varied between 0 and 0.3 mA, and between 0 and 1.3 mA. The fMRI activation maps of unsmoothed data, calculated using the box car function of the stimulus design as the correlate, were overlaid onto the corresponding GRE-EPI image of one time point (BrainVoyager QX 1.0 RC2, Brain Innovation, Maastricht, Netherlands).

Experiment 2 investigated the intensity of a single 1.56×1.56-mm^2 voxel (matrix size 128×128) in MR images as the current in the wire was adjusted to several different values during the 276-s-long time series.

The purpose of Experiment 3 was to study the ability of the phantom to mimic the generation mechanism of BOLD signals, i.e., spin dephasing. The images were acquired with a matrix size of 128×128. The phantom current was adjusted to 41 different values, and 10 scans (to be averaged) were performed at each step. First, the current flowed in one (say, positive) direction and was diminished step-by-step once every 30 s until it reached zero. Then it was increased in the opposite direction. At the end, it was again lowered and finally reversed in larger steps. Two analyses were made: First, the total signal intensity of the voxels crossing the phantom wire in the phase-encoded direction was plotted as a function of time and, thus, as a function of phantom current; the 10 voxels span the width of the phantom plus one voxel in both margins. Second, the ROI was enlarged to 10×10 voxels, now including the whole phantom interior plus margins.

3. Results

Fig. 3 shows the results of Experiment 1. The activations are thresholded at 5% false discovery rate (FDR), and the color scales indicate the Bonferroni-corrected *P* values of *t*-statistics. In the left panel ($I_{high}-I_{low}$=0.3 mA), the simulated activation is limited to one pixel in the image plane. On the right, the stronger current ($I_{high}-I_{low}$=1.3 mA) activates several voxels.

The sensitivity of the measurements to detect activations depends on the signal-to-noise ratio. Thus the decrease in signal due to susceptibility-based field inhomogeneities near the structures of the phantom might reduce the activation spread and intensity. The activation map with one activated voxel was, however, relatively resistant upon varying the statistical threshold: the indicated voxel remained the only activation between threshold levels of *q*(FDR) from 0.03 to

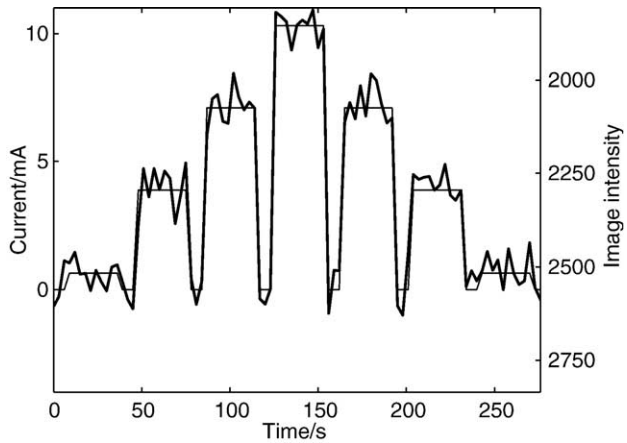

Fig. 4. Intensity (thick line) of the MR image in a single voxel as a function of the control current (thin line) during a 276-s recording during which four different current levels were applied. The image intensity axis is presented bottom up.

0.28. At q(FDR)>0.29, a voxel of opposite correlation polarity "became active". The next activated voxel was found at a level of statistical significance where half of the observed activations were false positives. Additionally, applying a three-dimensional spatial Gaussian filter of 4 mm (full width at half maximum) removed positive correlations when q(FDR)<0.50.

In the high-current case, too, applying the same spatial filter removed the positive correlation when q(FDR)<0.16. These observations on the response of the activations to the spatial filter relate to the aforementioned partial volume effects, whose consequences for the phantom are summarized in the Discussion.

Fig. 4 illustrates that in Experiment 2 the image intensity of the voxel followed linearly the current level in the wire. In the figure, the current levels are so high that even visual inspection easily reveals differences between the different conditions.

Fig. 5 visualizes the results of Experiment 3. The total signal intensity of the ROI composed of 10 successive voxels in the phase-encoded direction follows the solid line as the current applied in the phantom was adjusted according to the pattern shown at the bottom of the figure. The dashed line depicts, similarly, the total signal intensity of the ROI of 10×10 voxels. These plots show decreasing trends in signal level when the absolute value of the current increases (notice that the $|I|$ actually decreases during the first 240 s).

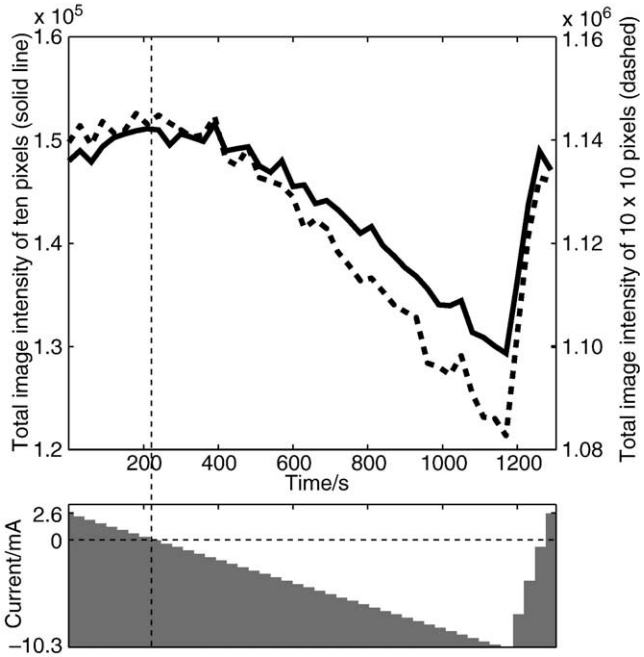

Fig. 5. Image intensities (upper graph) and the current level in the wire (lower graph) as a function of time. The solid line shows the total image intensity of a 1.6×15.6-mm^2 ROI (one voxel in frequency-encoded direction times 10 voxels in the phase-encoded direction) containing the phantom at the wire cross section in the image plane. The dashed line illustrates the total image intensity of a 15.6×15.6-mm^2 ROI. At each current level, 10 GRE-EPI images were scanned. Note the different scales for the averaged values within the two ROIs.

4. Discussion

We have demonstrated the principle, design and performance of a novel current phantom for simulating fMRI signals. Our phantom exploits a different mechanism than the BOLD contrast, but for the scanner and the whole analysis procedure, these two distortions affect the effective transverse relaxation time of the magnetization vector within a voxel in a similar way.

Our fMRI phantom, consisting of a wire within a material rich in MR-active nuclei, successfully created contrast in fMRI imaging with a GRE-EPI sequence. The average signal intensity change between the 0.3- and 0-mA current levels was 0.9%, which is on a par with many BOLD fMRI studies at 3 T (typical signal changes, 1–3% [14]) and could thus act as a template for studying BOLD activations.

In some cases (for example, in Fig. 3), two voxels on the border of the phantom in the high-current case were positively and statistically significantly correlated with the inducing current. The reason is that the phantom is too narrow for an activation simulation with induction current that is high. Substantial fractions of the volumes of the voxels on the border are either air- or polymethylacrylate-filled and thus do not contribute to MR signal. Even a slight misregistration may therefore drastically increase the signal apparently emerging from those voxels, and the tails of the induced magnetic fields may cause the positive correlation.

This signal spread is not, however, very problematic, because it can be tackled in several ways. First, decreasing the current in the wire reduces the activation of the border linearly (the current can be limited so that the border remains "nonactivated", while still retaining signal level changes comparable to BOLD response in the medium). Second, increasing the diameter of the phantom decreases the extraneous magnetic field distortion at the border with inverse square dependence on the distance from the wire. The most efficient way is, however, to ignore the border from analysis as it is known a priori to be irrelevant for the data. Additionally, spatial smoothing, as discussed above for the wire, is a plausible method for correcting the edge misregistration.

In Experiment 3, we demonstrated that the total signal within the ROIs decreased with application of increasing current. The first of the two ROIs selected encompassed the whole phantom in the phase-encoded direction and the second in the whole image plane. Outside the ROIs, in the respective dimensions, the signal level did not exceed the background noise, i.e., possibly misregistered voxels stayed within the ROIs. Thus, the signal void caused by the current-induced B_z, perceivable in Fig. 5, corresponds to dephasing of the spins, because all misregistered voxels

nonetheless belong to the ROIs and their signals are added to the grand total of the ROIs.

4.1. Possible applications

The usefulness of the fMRI phantom for the applications hinted in this paper remains to be experimentally proved. The following paragraphs outline some of the most promising applications.

Day-to-day variation of the same individual's BOLD signals is a well-acknowledged problem in cognitive fMRI studies. The constructed fMRI phantom could be used as a reference source during an fMRI study by introducing a periodic current pattern into the wire, while fMRI is simultaneously performed on a human subject. Thus it would be possible to decide whether some observed but unexpected behavior in the fMRI data has physiological or hardware-dependent origin. This use does not suffer from the sensitivity of individual voxel intensities to in-plane shifts.

The use of the fMRI phantom could also complement the method of Weisskoff [6] in monitoring system stability; this method uses multiple images of a phantom and evaluates the stability of signal intensity as a function of the size of the ROI. With the fMRI phantom, the signal changes introduced by the current could be monitored simultaneously with background signal, thus allowing the assessment of sensitivity to signal changes and noise separately. The method does not depend on the accurate prescription of the image plane with respect to the phantom's wire, although it is possible for this application.

Moreover, the fMRI phantom could be used to bring different measurements into agreement. Producing a certain signal in the wire during different fMRI experiments, for example, time-locked to stimuli presented to the subjects, gives a signal that acts as a basis for normalization of activation intensity; consequently, the variability of fMRI experiments performed on different sessions, days and individuals can be reliably assessed. The artificial phantom-produced fMRI activations could also be used to compare the measurements carried out with different scanners, e.g., as a yardstick to calibrate the scanners of multi-site consortia. In addressing scanners with different field strengths, one has to note that the susceptibility-related contrast diminishes with decreasing field strength, whereas the magnetic flux density produced by the fMRI phantom remains the same regardless of the external field. A method to ascertain the level of the output of the simulator might require the imaging of additional short series: the output of the simulator should be sampled by varying the slice positioning from the console to encompass the spatial variation of the size of one voxel, which would enable practically identical phantom setups in different measurements.

The phantom could be used in testing imaging sequences, both in choosing parameters for existing sequences and in designing new ones. While a proof with live subjects might be desired, the fMRI phantom could be used to provide data indicative of the quality of design choices. The phantom is, of course, indifferent to measurement conditions and habituation and could, consequently, be more reliable than human subjects in sequence research and development.

To sum up, we designed, constructed and tested an fMRI phantom. We successfully created "fMRI activations" that were readily retrieved with regular fMRI analysis software. With the 3-T MRI equipment, we were able to produce artificial activations remaining within one voxel in the image plane. Thereby we obtained a threshold for *t*-statistics, under which the point spreads of activation intensities are confined within one in-plane voxel. A number of uses for the simulator were conveyed.

Acknowledgments

The work was financially supported by the Jenny and Antti Wihuri Foundation and by the Academy of Finland. We thank Prof. Raimo Sepponen for discussions and Dr. Antti Tarkiainen for comments on the manuscript.

References

[1] Pauling L, Coryell CD. The magnetic properties and structure of hemoglobin, oxyhemoglobin and carbonmonoxyhemoglobin. Proc Natl Acad Sci U S A 1936;22:210–6.
[2] Ogawa S, Lee TM, Kay AR, Tank DW. Brain magnetic resonance imaging with contrast dependent on blood oxygenation. Proc Natl Acad Sci U S A 1990;87:9868–72.
[3] Schmitt F, Stehling MK, Turner R. Echo-planar imaging: theory, technique and application. Berlin: Springer-Verlag; 1998.
[4] Logan BR, Rowe DB. An evaluation of thresholding techniques in fMRI analysis. NeuroImage 2004;22:95–108.
[5] Sorenson JA, Wang X. ROC methods for evaluation of fMRI techniques. Magn Reson Med 1996;36:737–44.
[6] Weisskoff RM. Simple measurement of scanner stability for functional NMR imaging of activation in the brain. Magn Reson Med 1996; 36:643–5.
[7] Joensuu R, Renvall V, Hari R. FMRI phantom for an MR imager. Proceedings of the 10th Annual Meeting of the Organization for Human Brain Mapping, Budapest, Hungary, 2004. CD-ROM (abstract).
[8] Zhao Q, Duensing G, Fitzsimmons J. Development of smart phantom for characterizing fMRI informatics tools. Proc Intl Soc Mag Reson Med 2003;11:1834 (abstract).
[9] Scott GC, Joy MLG, Henkelman RM. In vivo detection of applied electric currents by magnetic resonance imaging. Magn Reson Imaging 1989;7:89–94.
[10] Bodurka J, Jesmanowicz A, Hyde JS, Xu H, Estkowski L, Li S-J. Current-induced magnetic resonance phase imaging. J Magn Reson 1999;137:265–71.
[11] Glowinski A, Adam G, Bücker A, Neuerburg J, van Vaals JJ, Günther RW. Catheter visualization using locally induced, actively controlled field inhomogeneities. Magn Reson Med 1997;38:253–8.
[12] Spees WM, Yablonskiy DA, Oswood MC, Ackerman JJH. Water proton MR properties of human blood at 1.5 tesla: magnetic susceptibility, T_1, T_2, T_2*, and non-Lorentzian signal behavior. Magn Reson Med 2001;45:533–42.
[13] Marciani L, Ramanathan C, Tyler DJ, Young P, Manoj P, Wickham M, et al. Fat emulsion measured using NMR transverse relaxation. J Magn Reson 2001;153:1–6.
[14] Krüger G, Kastrup A, Glover GH. Neuroimaging at 1.5 T and 3.0 T: comparison of oxygenation-sensitive magnetic resonance imaging. Magn Reson Med 2001;45:595–604.